Mersin Photogrammetry Journal
https://dergipark.org.tr/en/pub/mephoj
e-ISSN 2687-654X

Effect of denoising methods for hyperspectral images classification: DnCNN, NGM, CSF, BM3D and Wiener

Mehmet Akif Günen [*1], **Erkan Besdok** [2]

[1]*Gümüşhane University, Department of Geomatics Engineering, Türkiye*
[2]*Erciyes University, Department of Geomatics Engineering, Türkiye*

Keywords
Denoising
Remote sensing
Hyperspectral
Classification

Research Article
DOI:10.53093/mephoj.1213166

Received:01.12.2022
Revised:23.02.2023
Accepted:27.02.2023
Published:27.05.2023

Abstract

Hyperspectral images are widely used for land use/cover analysis in remote sensing due to their rich spectral information. However, these data often suffer from noise caused by various factors such as random and systematic errors, making them less useful for end-users. In this study, denoising methods (i.e., DnCNN, NGM, CSF, BM3D, and Wiener) for hyperspectral images were compared using the Pavia University hyperspectral dataset with four different noise types: Gaussian, Salt & Pepper, Poisson, and Speckle. After denoising, the k-nearest neighbor method was used to classify the image, and statistical and visual performance comparisons were performed on the classified data. Six performance metrics -Accuracy, Sensitivity, Specificity, Precision, F-Score, and G-Mean- were employed to compare the outcomes qualitatively. The findings demonstrate that DnCNN and BM3D have the best outcome performance for all four noise types. Due to their lack of sensitivity and specificity, the CSF and Wiener approaches had low performance for particular noise sources. For all noise types, the NGM approach had the worst results. The validated instruments not provide effective results when it came to denoising Salt & Pepper noise, but they managed to produce outstanding results when it came to denoising Poisson noise. In order to enhance the quality and usability of hyperspectral images for land use/cover analysis, this study emphasizes the significance of choosing an effective denoising technique.

1. Introduction

Hyperspectral images (HSI) are significant data that can be successfully employed in many different industries, such as agriculture, astronomy, and the military, including remote sensing and photogrammetry, because they contain significantly more spectral information than three-band red, green, and blue (RGB) images. The number of photons captured per band is much lesser in HSIs than in RGB images, allowing different noises to be easily incorporated into the corresponding bands during the acquisition process. This is because HSIs capture the spectral information of each spatial location in a scene with large wavebands [1-3]. These noises cause image distortions, which have a detrimental effect on the performance of all HSI applications as well as how the HSI is visually presented. An important stage in the analysis and processing of HSI is denoising. The multi-detector imaging method of HSI sensors, however, results in complex noises like random noise and structural stripe noise. Through advanced analysis, this complex noise condition dramatically affects the ability to extract and comprehend information. Unwanted signals and marks on the image are collectively referred to as noise from images, and they frequently contaminate images and provide a hazy impression. Depending on how they impact the image, the noises have different distributions. The noise must be identified based on its pattern and probabilistic properties. Image and signal data include a wide variety of noise [4-6]. Gaussian, Salt & Pepper, Poisson, impulse, and Speckle noise are the most common types of noise that distort images. Effective image denoising is essential in the majority of image processing applications since the performance of subsequent image processing operations completely depends on how well the noise reduction process performs. However, this is a challenging task because the denoising operator must effectively remove

* **Corresponding Author**
*(akif@erciyes.edu.tr) ORCID ID 0000-0001-5164-375X
(ebesdok@erciyes.edu.tr) ORCID ID 0000-0001-9309-375X

Cite this article
Günen, M. A., Beşdok, E. (2023). Effect of denoising methods for hyperspectral images classification: DnCNN, NGM, CSF, BM3D and Wiener. Mersin Photogrammetry Journal, 5(1), 1-9

noise while preserving crucial information in the image. The majority of contemporary filtering algorithms employ sequential statistical filters that make use of the rank information of a sufficient collection of noisy input pixels [7]. Non-local means algorithm (NLM) [8], block matching and 3D filtering algorithm (BM3D) [9], residual learning of deep CNN for image denoising (DnCNN) [3], K-SVD algorithm [10], Markov random field models (MRF) [11], Non-Local Meets Global (NGM) [12], weighted nuclear norm minimization (WNNM) [13], Wiener [14], and a cascade of shrinkage field (CSF) [15] are some of the HSI noise removal approaches that have been presented in recent years.

Due to all of these factors, it is crucial to identify the denoising filter that is appropriate for each type of noise, making this study crucial. This study used the k-nearest neighbor approach to classify Gaussian, Salt & Pepper, Poisson, and Speckled HSI images after applying the DnCNN, NGM, CSF, BM3D, and Wiener filters. The effectiveness of the filtering techniques was compared.

The remainder of this work is structured as follows: Section 2 defines the material and method, Section 3 presents the results and discussion, and Section 4 includes the conclusion.

2. Material

In this study, various types of noise were added to the HSI and then the classification performance of the HSI was investigated by applying some noise removal methods. In this context, the flow chart of the study performed in Figure 1 is presented.

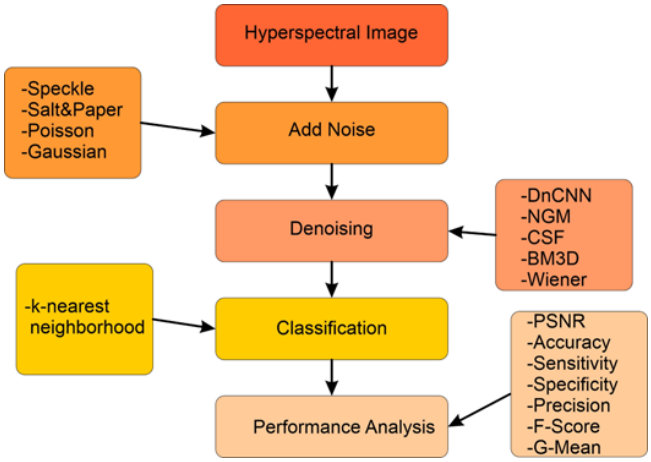

Figure 1. Flow chart of study

Pavia is a dataset acquired using the ROSIS sensor with a ground sampling distance of 1,3 m over the Italian city of Pavia. The dataset is divided into two parts: University of Pavia consist of 103 bands with 610x340 pixels and Pavia Center consist of 102 bands with 1096x715 pixels [16]. In Figure 2, RGB, ground truth and data cube representations of the Pavia University dataset are given.

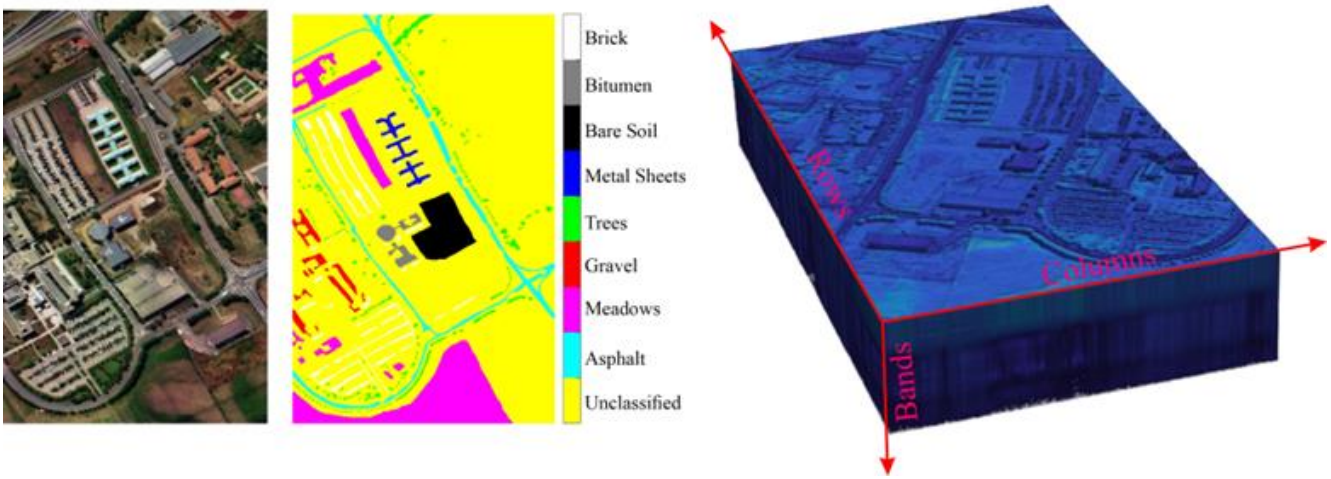

Figure 2. A representation of the RGB, ground truth, and hyperspectral data cube of Pavia HIS

There are various urban elements in Pavia (such metals, bricks, and asphalt etc.). Nine different areas of interest were recognized, making up 50% of the surface. Due to its dimension and ability to assess the usage of HSI for possible applications, this dataset has long been regarded as one of the primary references. Preprocessing may be essential to eliminate some pixels that lack spectral information. The class distribution of the Pavia University data set used in this study is presented in Table 1.

The implementation was carried out using MATLAB 2022a software on a laptop with AMD Ryzen 9 5900HX Radeon 3.30 GHz processor, 32 Gb RAM and AMD Radeon RX 6700M graphics card.

Table 1. Pavia dataset specifications

#	Class Name	Ground Sample
1	Asphalt	6631
2	Meadow	18649
3	Gravel	2099
4	Trees	3064
5	Painted Metal Sheet	1345
6	Bare Soil	5029
7	Bitumen	1330
8	Self-Blocking Brick	3682
9	Shadow	947

3. Methods

In this section, noise types, denoising methods and classification method (i.e., k-nearest neighbor), which form the basis of the proposed method, are explained.

3.1. Noise types

Noise is commonly defined in digital images as a random change in brightness or color information, and it is frequently generated randomly or systematically by the technological constraints of the image acquisition sensor and improper ambient conditions. Furthermore, noise may penetrate the image in a variety of ways during image collecting and transmission. Noise in an image can be either additive or multiplicative. An additional noise signal is added to the original image in the additive noise model to produce a distorted noise image/signal. The original image is multiplied by noise in the multiplicative noise model, but in the additive noise model, the noise is added to the original image to create a distorted noisy image or signal [17-19]. In general, this process can be described as Equation 1.

$$f(x, y) = a(x,y) + b(x,y) \text{ or } f(x, y) = a(x,y) \times b(x,y) \quad (1)$$

(x, y) represents the pixel position, $a(x, y)$ represents the original image, the noise inside the distorted/noise, $b(x, y)$, added image is represented by $f(x, y)$.

Gaussian noises, in which the statistical behavior of random variables is characterized by a probability density function, are typically induced by insufficient illumination conditions, atom thermal vibration, and the discontinuous nature of warm object radiation. Gaussian noise is distributed uniformly throughout the signal. A noisy image is a set of pixels formed by adding the original pixel values to a random Gaussian noise value. A Gaussian's probability distribution function has the shape of a bell. The most typical application for Gaussian noise is white Gaussian noise. The magnitude of the Gaussian Noise rises proportionally to the standard deviation (σ). Salt & pepper noise, also known as impulse noise, appears as black and white dots in the digital image. This model, also referred to as data drop noise, statistically reduces the original data values. Only a few pixels are extremely noisy and are thus generated by dust particles from overheated components in the image acquisition source. This noise occurs in the image as a result of sharp and rapid oscillations in the image signal, and only those few pixels are extremely noisy. Poisson noise appears due to the stochastic nature of electromagnetic waves, including visible light, gamma rays, and x-rays. The non-linear response of image sensors and recorders generates Poisson noise. The image-related term is considered to have its standard deviation because the mean and variance of a Poisson distribution are the same, assuming the variance of the noise is one. Speckle noise, unlike other types of noise, is multiplicative noise. It degrades image quality by simulating a backscattered wave created by diffuse reflection. This form of noise is commonly found in synthetic aperture radar images used in remote sensing investigations, making it difficult for practitioners to detect minute features [20-23].

3.2. Denoising methods

The problem of noisy data, which is often unavoidable in real-world applications, has become a widespread issue that must be addressed with appropriate denoising techniques [24]. Denoising an image is a complex procedure since noise is dependent on the image's high-frequency content. In general, the objective is to achieve a compromise between suppressing noise as much as feasible while losing as little information as possible. Image noise can be removed using filter-based methods such as mean, median, wavelet, or Wiener. Modern approaches, however, have begun to be employed more frequently as computer technology has gained access to high hardware capabilities. Modern approaches such as Deep CNN Residual Learning (DnCNN), Non-local Meets Global (NGM), a cascade of shrinkage fields (CSF), block-matching and 3-D filtering (BM3D), and Wiener methods were used in this study to denoising.

Deep neural networks have made various attempts to address the denoising issue. CNN have recently demonstrated outstanding effectiveness in handling a variety of vision tasks, largely because to the ease of access to large-scale datasets and the advancements in deep learning techniques. DnCNN, a model that has been proposed to handle a variety of low-level tasks, not only resolves issues with image denoising, JPEG block removal, and super resolution, but it also carries out a blind reconstruction without knowing anything about the input image. The VGG network is used by DnCNN to construct the network architecture. 400 images are used to train a network and it is claimed that the residual image is easier to learn than the noisy image. The used DnCNN network has 59 layers. The residual learning formulation is used in the DnCNN model. In contrast to the residual network, which makes utilization numerous residual units, DnCNN only uses one residual unit to estimate the residual image. Additionally, DnCNN's incorporation of batch normalization and residual learning can lead to quick and consistent training as well as improved denoising performance [3]. The MATLAB code for DnCNN can be found at https://github.com/cszn/DnCNN.

The NGM approach [25] was developed for HSI denoising. In order to combine spatial nonlocal similarity and global spectral low-order feature in NGM, the complex HSI denoising paradigm is implemented. From the noisy HSI, first the low-dimensional orthogonal base and its associated reduced image are learned, and then the reduced image and orthogonal base are updated by spatial nonlocal noise removal and recursion regularization, respectively. MATLAB code is available at https://github.com/quanmingyao/NGMeet.

In the CSF method, shrinkage fields, an image restoration architecture derived from existing

optimization algorithms for common random field models, are introduced and combined the random field based model and the unfolded quasi-quadratic optimization algorithm in a single learning framework [15]. The MATLAB code for CSF can be found at https://github.com/uschmidt83/shrinkage-fields.

BM3D proposed by Dabov et al., [26] proposes new image noise removal strategy based on improved sparse representation in the transform domain, and in BM3D, non-local similar patches are adaptively searched twice in a local widow of size 25x25, and thus the final effective patch size is 49x49. Increasing sparsity is accomplished by combining related 2D image segments into 3D data arrays known as groups. BM3D's MATLAB code may be found at https://webpages.tuni.fi/foi/GCF-BM3D/.

There are several classic strategies, but the most basic approach, the Wiener filter, is a linear estimator that minimizes the mean square error between the original and noisy data. It is defined in various ways and utilized in diverse situations. When using a low-pass filter to blur an image, reverse filtering can be used to restore the image. The Wiener filter, developed by Norbert Wiener in 1940, reduces extra noise by conducting an efficient trade-off between reverse filtering and noise smoothing. However, because reverse filtering is particularly sensitive to extra noise, Wiener filtering reverses blur at the same time [24, 27].

3.3. k-nearest neighbor method

One of the most widely used supervised classification methods is the k-nearest neighbor method. Cover and Hart's technique essentially uses k-nearest neighbor pixels for classification [28]. The query pixel is assigned to the class where the predominance is close after first determining the k-nearest neighborhood and measuring the query sample's distance from the training data using distance functions like Cosine, Euclidean, Manhattan, or Minkowski. The training process for the k-closest approach is carried out using training data. The approach makes selecting the best k value rather difficult [29].

4. Results and Discussion

In this study, gaussian, Salt & Pepper, Poisson and Speckle noises were added to the Pavia University dataset. Then, DnCNN, NGM, CSF, BM3D and Wiener denoising methods were applied to the contaminated images and the results were compared statistically. RGB images with noise added are presented in Figure 3.

Figure 3. RGB image of HSI with noise added a) Speckle, b) Salt & Pepper, c) Poisson and d) Gaussian

While performing the noise addition, $\sigma^2 = 0.01$ for Gaussian noise, $d = 0.02$ for Salt & Pepper noise, $\mu = 10$ for Poisson noise and $\sigma^2 = 0.1$ for Speckle noise. The RGB images of the HSIs in which the denoising process is applied after the noise addition are presented in Figure 4. After denoising, the HSI was classified using the k-nearest neighbor method. Before classification, the data set was randomly divided into 30% test and 70% training dataset. A Support Vector Machine could also be used for classification, but due to the dimensionality problem, these algorithms require a lot of workload equipment. In their study, Singh et al., [30] showed that the k-nearest neighbor method provides the most accurate result after support vector machines in HSI classification. Experimental application was carried out using the parameters used in [30]. In this context, cosine distance functions, 10 nearest neighbor number (k) and equal distance weight parameters are preferred. When looking at Figure 4, it is clear that the impacts of Gaussian noise on RGB cannot be totally avoided, particularly for BM3D and Wiener. Furthermore, the influence of salt & pepper noise cannot be seen removed for DnCNN and Wiener. The CSF approach resulted in texture softening, particularly in structures with sharp corners and areas of land type change. By changing the density difference of objects with varying reflectance values, the NGM approach has made it more visible.

In terms of noise types, BM3D, an effective and powerful extension of the non-local averaging method, generated extremely consistent findings. BM3D is a two-stage, non-local filtering approach in transform space in which related patches are stacked in 3D groups and then transformed into wavelet space using block mapping. The wavelet domain is then used for coefficient Wiener filtering. Because peak-signal-to-noise ratio (PSNR) does not always guarantee an improvement in the visual effect, Figure 5 shows an overlay of the denoised and classified with k-nearest neighbor of HSI on the RGB image.

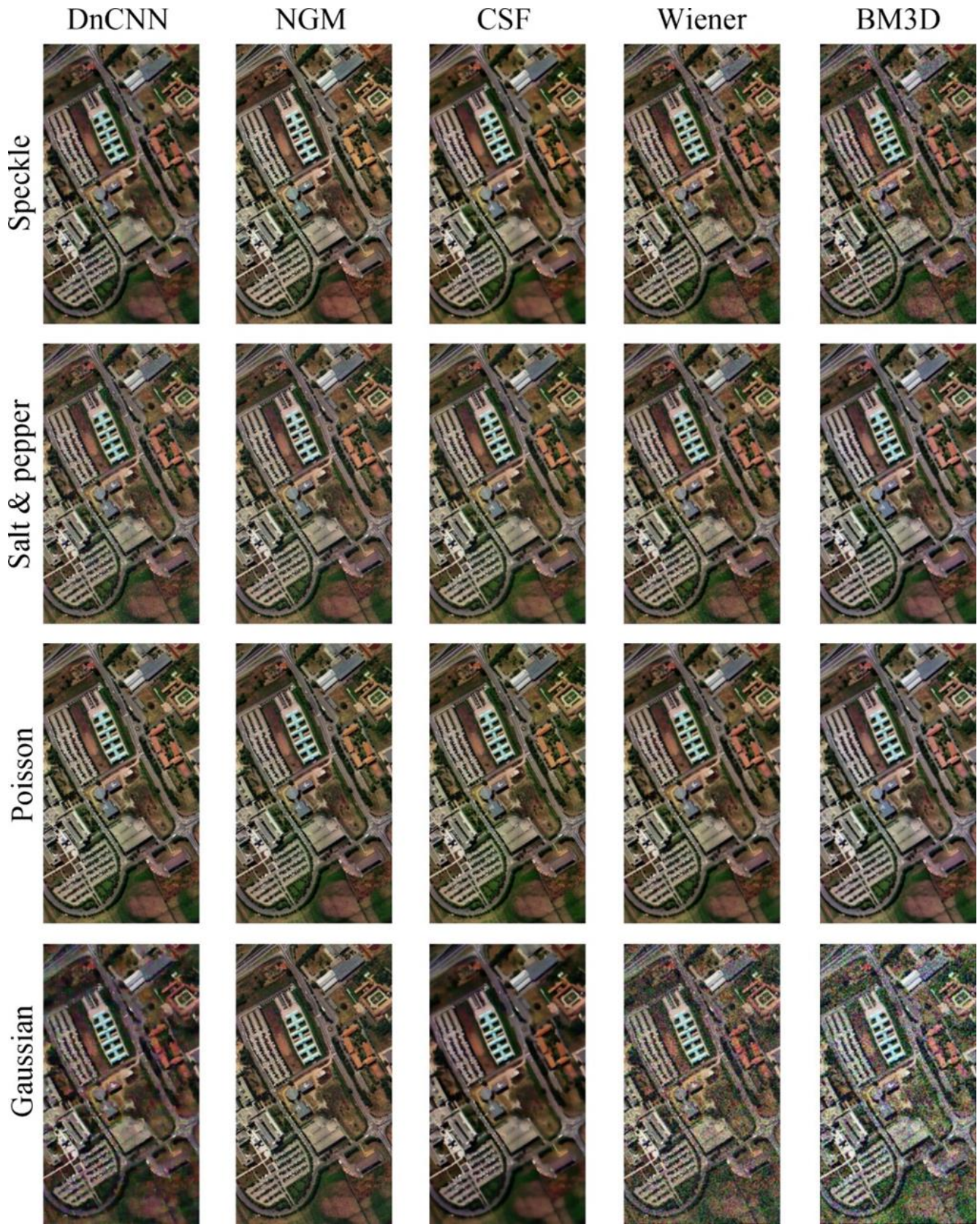

Figure 4. Denoising results of HSI exposed to various sources of noise

Many analyses were carried out using the ground truth data from the classified images. Figure 6 shows the PSNR results of denoising based on ground truth data. In statistical comparisons, the accuracy metric alone does not yield useful conclusions. The distribution of the data sets in Table 1 shows that the meadow areas have more samples than the shadow areas. The usage of various metrics in unbalanced data sets is required as a result.

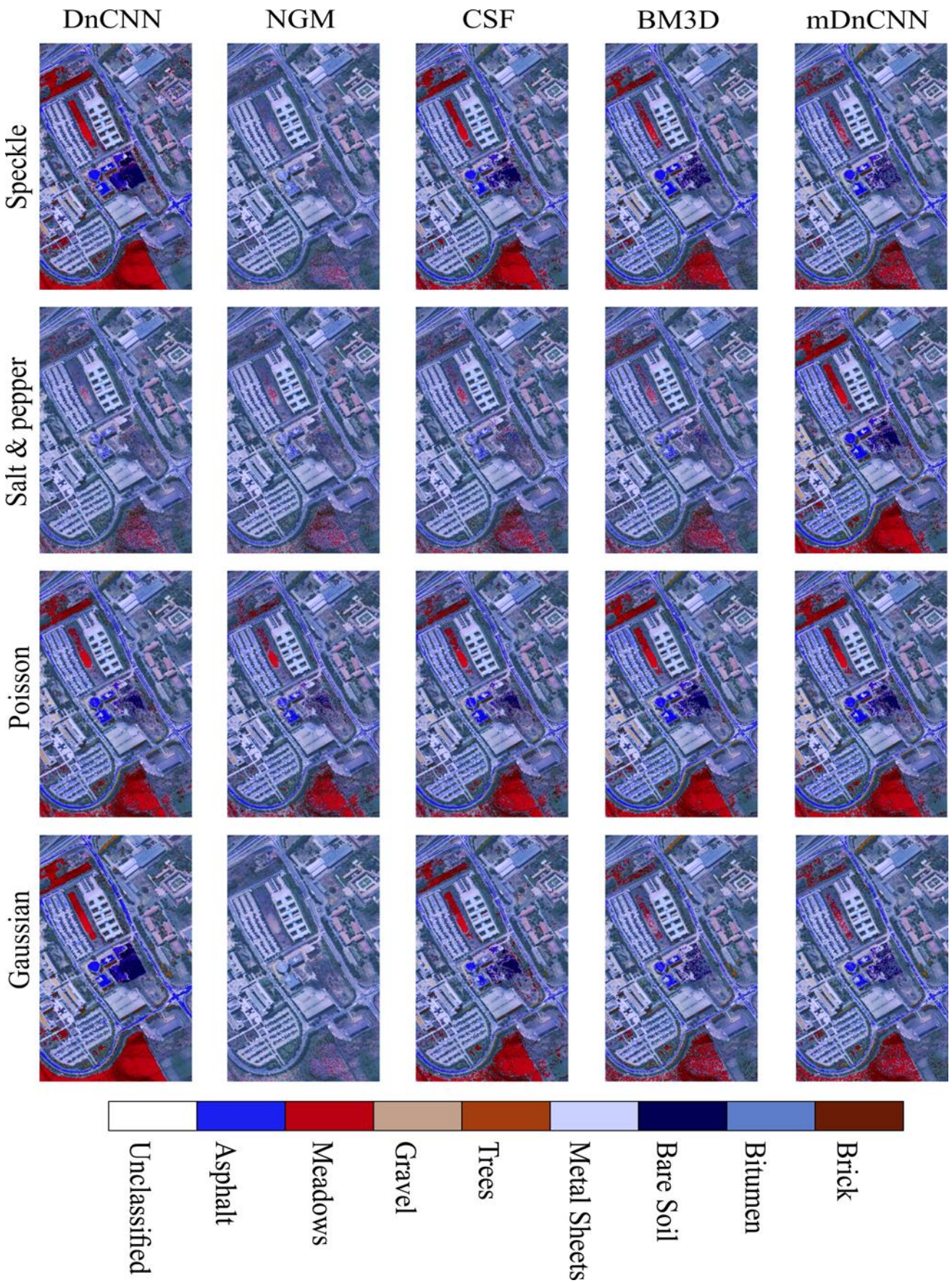

Figure 5. Overlaid classification results on RGB image

The performance of five distinct denoising filters (i.e., DnCNN, NGM, CSF, Wiener, and BM3D) was compared for four different types of noise (i.e., Speckle, Salt & Pepper, Poisson, and Gaussian) in the following Table 2. For each filter, the six-performance metrics -accuracy, sensitivity, specificity, precision, F-Score, and G-Mean- were calculated. With Salt & Pepper noise, the accuracy metrics obtained by Wiener and NGM are reasonably comparable, however the specificity and G-mean values demonstrate that the methods produce different results.

The fact that NGM produces the worst result especially for the Salt & Pepper method shows that the method is ineffective against this noise. NGM produces more effective sensitivity results for Poisson noise than other types of noise. In general, approaches other than the BM3D method could not produce very effective results with Salt & Pepper noise, while all methods could effectively produce results with Poisson noise.

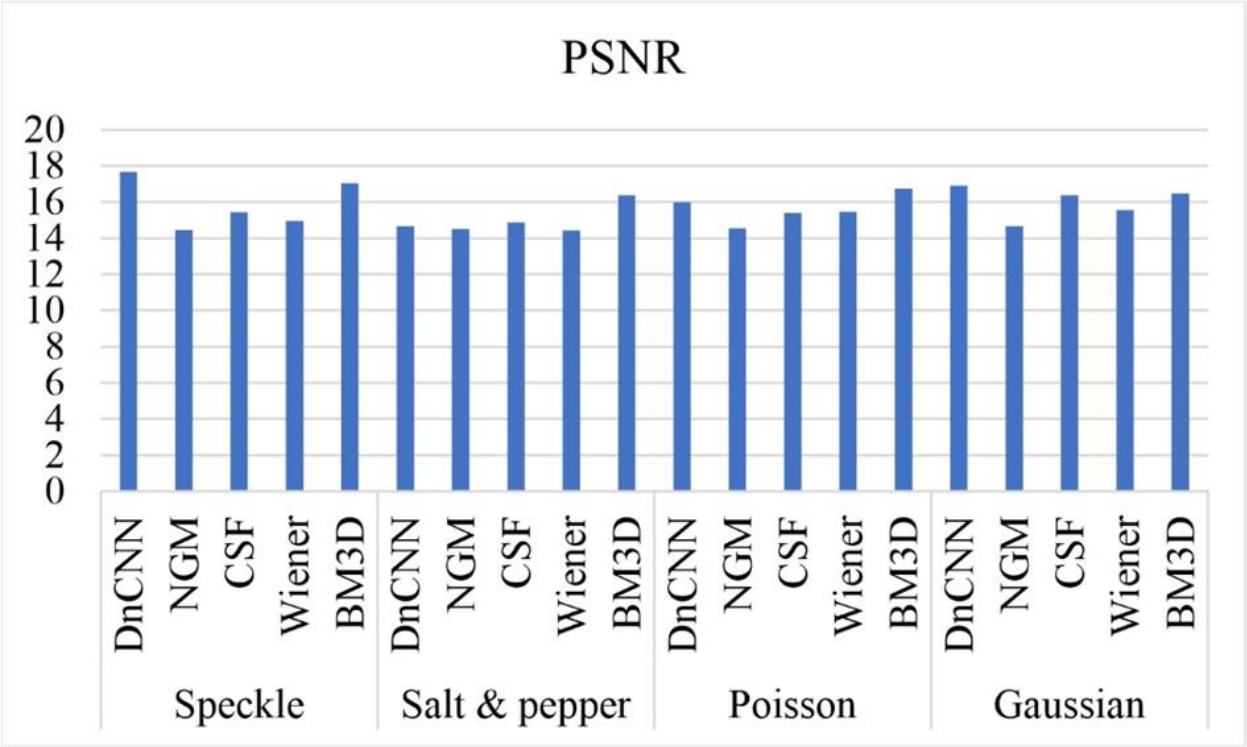

Figure 6. PSNR value based on the Pavia dataset

Table 2. Statistical results calculated according to the Pavia dataset (*Bold marked indicated best result)

		Accuracy	Sensitivity	Specificity	Precision	F-Score	G-Mean
Speckle	DnCNN	**93.20**	96.68	**78.70**	**94.84**	**95.75**	**87.88**
	NGM	79.74	96.76	14.15	81.33	88.37	36.16
	CSF	85.20	93.78	50.05	88.34	90.98	69.70
	Wiener	85.45	90.94	55.14	90.79	90.86	76.33
	BM3D	89.35	**98.39**	62.06	89.27	93.61	73.35
Salt & Pepper	DnCNN	80.16	**98.99**	10.43	80.48	88.78	28.22
	NGM	79.25	96.85	10.62	80.86	88.14	32.23
	CSF	81.93	94.49	33.12	84.60	89.27	55.87
	Wiener	79.00	97.30	7.21	80.41	88.06	27.40
	BM3D	**88.62**	93.57	**64.59**	**92.19**	**92.88**	**80.74**
Poisson	DnCNN	87.53	96.06	57.27	89.07	92.43	72.59
	NGM	79.94	**96.31**	16.85	81.73	88.42	39.49
	CSF	84.30	94.08	45.48	87.20	90.51	65.93
	Wiener	86.08	94.84	52.22	88.49	91.55	70.20
	BM3D	**89.47**	94.93	**66.43**	**92.04**	**93.46**	**80.67**
Gaussian	DnCNN	**89.75**	**98.65**	**63.51**	89.5	**93.85**	**74.11**
	NGM	80.83	96.07	22.93	82.65	88.86	45.42
	CSF	88.30	94.16	62.36	**91.39**	92.76	78.51
	Wiener	86.00	95.70	50.51	87.80	91.58	67.95
	BM3D	88.05	98.17	56.60	88.12	92.87	69.57

It is an important result that DnCNN produces effective results in Speckle noise as well as Gaussian. By learning the residual noise rather than the denoised image directly, researchers suggested [3] to denoise natural images using additive Gaussian noise using DnCNN. Similar research has been used as the foundation for various image processing networks, including Speckle de-noising [31] and the detection of illness in tomato leaves [32]. However, the disadvantage of vanishing gradients, which can happen with very deep networks, is reduced via residual learning. In contrast to other methods, NGM performs well just in the sensitivity criterion and poorly in the other criteria. This suggests that NGM is not the ideal choice for various sorts of noise. While the CSF method shows lower performance in sensitivity and specificity criteria compared to other

methods, it shows high performance against other criteria. This indicates that CSF may give less accurate results than other methods. The Wiener technique performs moderately in all noise types; however, it performs poorly by the G-mean criterion when compared to other methods. This indicates that, in many situations, the Wiener technique tends to produce less reliable result than other methods.

5. Conclusion

Denoising in multidimensional images has recently grown in popularity as a study area with potentially significant applications. This paper discusses the issue of denoising in high-dimensional remote sensing images and evaluates the effectiveness of five distinct approaches. Four additional noises have been added in this situation, and HSI has been classified. Denoising performance can be defined by high benchmarks. Looking at the quantitative and qualitative results, the BM3D filter generally outperformed other filters. In particular, the BM3D filter for Salt & Pepper and Gaussian noise had the highest G-Mean, with a higher accuracy, sensitivity, specificity, precision, and F-Score than the other filters. Denoising techniques performed better against Poisson noise even though they were statistically ineffective against Salt & Pepper noise. The DnCNN filter performed better than other filters for Gaussian and Salt & Pepper noises, but failed for Poisson and Speckle noises. NGM and Wiener filters performed the worst for all noise types. The low specificity of the NGM filter and the low sensitivity of the Wiener filter are particularly notable. As a result, evaluating the performance of different denoising filters for different noise types aids in determining the optimum filter for a given application. In summary, this study highlights the importance of selecting an appropriate denoising method for hyperspectral images to improve their quality and usability for land use/cover analysis. The results suggest that DnCNN and BM3D are the most effective methods for denoising hyperspectral images, while the CSF, Wiener, and NGM approaches have limitations and may not be suitable for certain noise types.

The main advantage of this research is the comparison of a diverse variety of HSI noise reduction techniques to identify the most successful approach. The performance of various approaches has been evaluated using a variety of situations and criteria. The disadvantage of working with HSI data is that processing the data is difficult because of the enormous amount of data dimensionality, the requirement for a big data set, and the requirement to select parameters for the classification technique and filters. For these reasons, methods will be tested on various data sets (such as Salinas A, Indian Pines, and Botswana, etc.) in future studies. The effectiveness of filtering methods according to different data dimensions will also be investigated. Because a thorough investigation is needed to determine how different feature reduction techniques (i.e., Principal component analysis, Linear discriminant analysis, and minimum redundancy maximum relevance etc.) affect the outcome.

Author contributions

Mehmet Akif Günen: Conceptualization, Validation, Visualization, and Investigation **Erkan Beşdok:** Writing, Reviewing and Editing.

Conflicts of interest

The authors declare no conflicts of interest.

References

1. Günen, M. A., Atasever, U. H., & Beşdok, E. (2020). Analyzing the contribution of training algorithms on deep neural networks for hyperspectral image classification. Photogrammetric Engineering & Remote Sensing, 86(9), 581-588.
2. Nofrizal, A. Y., Sonobe, R., Hiroto, Y., Morita, A., & Ikka, T. (2022). Estimating chlorophyll content of Zizania latifolia with hyperspectral data and random forest. International Journal of Engineering and Geosciences, 7(3), 221-228.
3. Zhang, K., Zuo, W., Chen, Y., Meng, D., & Zhang, L. (2017). Beyond a gaussian denoiser: Residual learning of deep cnn for image denoising. IEEE transactions on image processing, 26(7), 3142-3155.
4. Lam, A., Sato, I., & Sato, Y. (2012, November). Denoising hyperspectral images using spectral domain statistics. In Proceedings of the 21st International Conference on Pattern Recognition (ICPR2012) (pp. 477-480). IEEE.
5. Annam, S., & Singla, A. (2020, November). Correlative analysis of denoising methods in spectral images embedded with different noises. In 2020 Sixth International Conference on Parallel, Distributed and Grid Computing (PDGC) (pp. 318-323). IEEE.
6. Momeny, M., Jahanbakhshi, A., Neshat, A. A., Hadipour-Rokni, R., Zhang, Y. D., & Ampatzidis, Y. (2022). Detection of citrus black spot disease and ripeness level in orange fruit using learning-to-augment incorporated deep networks. Ecological Informatics, 71, 101829.
7. Yuksel, M. E., & Besdok, E. (2004). A simple neuro-fuzzy impulse detector for efficient blur reduction of impulse noise removal operators for digital images. IEEE Transactions on Fuzzy Systems, 12(6), 854-865.
8. Buades, A., Coll, B., & Morel, J. M. (2005, June). A non-local algorithm for image denoising. In 2005 IEEE computer society conference on computer vision and pattern recognition (CVPR'05) (Vol. 2, pp. 60-65). IEEE.
9. Dabov, K., Foi, A., Katkovnik, V., & Egiazarian, K. (2006, February). Image denoising with block-matching and 3D filtering. In Image processing: algorithms and systems, neural networks, and machine learning (Vol. 6064, pp. 354-365). SPIE.
10. Aharon, M., Elad, M., & Bruckstein, A. (2006). K-SVD: An algorithm for designing overcomplete dictionaries for sparse representation. IEEE Transactions on signal processing, 54(11), 4311-4322.
11. Li, S. Z. (2009). Markov random field modeling in image analysis. Springer Science & Business Media.

12. He, W., Yao, Q., Li, C., Yokoya, N., Zhao, Q., Zhang, H., & Zhang, L. (2020). Non-local meets global: An iterative paradigm for hyperspectral image restoration. IEEE Transactions on Pattern Analysis and Machine Intelligence, 44(4), 2089-2107.
13. Gu, S., Zhang, L., Zuo, W., & Feng, X. (2014). Weighted nuclear norm minimization with application to image denoising. In Proceedings of the IEEE conference on computer vision and pattern recognition (pp. 2862-2869).
14. Ghael, S., Sayeed, A. M., & Baraniuk, R. G. (1997, July). Improved wavelet denoising via empirical Wiener filtering. In SPIE Technical Conference on Wavelet Applications in Signal Processing.
15. Schmidt, U., & Roth, S. (2014). Shrinkage fields for effective image restoration. In Proceedings of the IEEE conference on computer vision and pattern recognition (pp. 2774-2781).
16. Günen, M. A., Atasever, U. H., & Beşdok, E. (2020). Analyzing the contribution of training algorithms on deep neural networks for hyperspectral image classification. Photogrammetric Engineering & Remote Sensing, 86(9), 581-588.
17. Yüksel, M. E., Baştürk, A., & Beşdok, E. (2004). Detail-preserving restoration of impulse noise corrupted images by a switching median filter guided by a simple neuro-fuzzy network. EURASIP Journal on Advances in Signal Processing, 2004(16), 1-11.
18. Çivicioğlu, P., Alçı, M., & Beşdok, E. (2004). Impulsive noise suppression from images with the noise exclusive filter. EURASIP Journal on Advances in Signal Processing, 1-7.
19. Beşdok, E. (2004). A new method for impulsive noise suppression from highly distorted images by using Anfis. Engineering Applications of Artificial Intelligence, 17(5), 519-527.
20. Kumar, N., & Nachamai, M. (2017). Noise removal and filtering techniques used in medical images. Oriental Journal of Computer Science & Technology, 10(1), 103-113.
21. Patidar, P., Gupta, M., Srivastava, S., & Nagawat, A. K. (2010). Image de-noising by various filters for different noise. International Journal of Computer Applications, 9(4), 45-50.
22. Kanagalakshmi, K., & Chandra, E. (2011, April). Performance evaluation of filters in noise removal of fingerprint image. In 2011 3rd International Conference on Electronics Computer Technology (Vol. 1, pp. 117-121). IEEE.
23. Niknejad, M., & Figueiredo, M. A. (2018, September). Poisson image denoising using best linear prediction: a post-processing framework. In 2018 26th European Signal Processing Conference (EUSIPCO) (pp. 2230-2234). IEEE.
24. Atasever, U. H., & Gunen, M. A. (2021). Change detection approach for SAR imagery based on arc-tangential difference image and k-Means++. IEEE Geoscience and Remote Sensing Letters, 19, 1-5.
25. He, W., Yao, Q., Li, C., Yokoya, N., & Zhao, Q. (2019). Non-local meets global: An integrated paradigm for hyperspectral denoising. In Proceedings of the IEEE/CVF Conference on Computer Vision and Pattern Recognition (pp. 6868-6877).
26. Dabov, K., Foi, A., Katkovnik, V., & Egiazarian, K. (2007). Image denoising by sparse 3-D transform-domain collaborative filtering. IEEE Transactions on image processing, 16(8), 2080-2095.
27. Juang, L. H., & Wu, M. N. (2010). Image noise reduction using Wiener filtering with pseudo-inverse. Measurement, 43(10), 1649-1655.
28. Cover, T., & Hart, P. (1967). Nearest neighbor pattern classification. IEEE transactions on information theory, 13(1), 21-27.
29. Günen, M. A. (2022). Performance comparison of deep learning and machine learning methods in determining wetland water areas using EuroSAT dataset. Environmental Science and Pollution Research, 29(14), 21092-21106.
30. Singh, S., Singh, D., Sajwan, M., Rathor, V. S., & Garg, D. (2022). Hyperspectral image classification using multiobjective optimization. Multimedia Tools and Applications, 81(18), 25345-25362.
31. Park, D. Y., & Park, J. H. (2020). Hologram conversion for speckle free reconstruction using light field extraction and deep learning. Optics Express, 28(4), 5393-5409.
32. Karthik, R., Hariharan, M., Anand, S., Mathikshara, P., Johnson, A., & Menaka, R. (2020). Attention embedded residual CNN for disease detection in tomato leaves. Applied Soft Computing, 86, 105933.